Kinetic Mechanism of Cytochrome c Folding: Involvement of the Heme and Its Ligands

ARTICLE *in* BIOCHEMISTRY · JULY 1994

Impact Factor: 3.02 · DOI: 10.1021/bi00188a023 · Source: PubMed

3 AUTHORS, INCLUDING:

Heinrich Roder
Fox Chase Cancer Center
121 PUBLICATIONS **8,484** CITATIONS

Kinetic Mechanism of Cytochrome *c* Folding: Involvement of the Heme and Its Ligands†

Gülnur A. Elöve,‡ Abani K. Bhuyan,‡,§ and Heinrich Roder*,‡,§

Institute for Cancer Research, Fox Chase Cancer Center, 7701 Burholme Avenue, Philadelphia, Pennsylvania 19111, and Department of Biochemistry and Biophysics, University of Pennsylvania, Philadelphia, Pennsylvania 19104

Received January 31, 1994; Revised Manuscript Received April 8, 1994®

ABSTRACT: The covalently attached heme and its axial ligands not only are essential for the structure and function of cytochrome *c* but they also play an important role in the folding process. Under typical denaturing conditions (concentrated guanidine hydrochloride or urea near pH 7), one of the axial ligands, His 18, remains bound to the oxidized heme iron, but the second ligand, Met 80, is replaced by a non-native histidine ligand (His 26 or His 33 in horse cytochrome *c*). Using quenched-flow and NMR methods, hydrogen exchange rates were measured for several individual amide protons in guanidine-denatured horse cytochrome *c*. The observation of a single highly protected (140-fold) backbone amide, that of His 18, suggests the presence of a persistent H-bond consistent with heme ligation of the His 18 side chain in the unfolded state. Heme absorbance changes induced by rapid acidification of oxidized cytochrome *c* in 4.5 M guanidine hydrochloride from pH 7.8 to 4.6 or below exhibit two kinetic phases with rates of 110 and 25 s^{-1}, attributed to the dissociation of non-native histidine ligands from the heme in the unfolded state. The kinetics of folding from guanidine-denatured cytochrome *c* under a variety of initial and final conditions was investigated by stopped-flow methods, using tryptophan fluorescence as a conformational probe and Soret absorbance as a probe for the ligation state of the heme. A fast kinetic phase (80 s^{-1}) accompanied by a major decrease in fluorescence and a minor absorbance change coincides with the formation of a partially folded intermediate with interacting chain termini detected in earlier pulsed NH exchange measurements [Roder, H., Elöve, G. A., & Englander, S. W. (1988) *Nature 335,* 700]. At neutral pH, an intermediate kinetic phase (1.8 s^{-1}) accounts for 78% of the absorbance change and 47% of the fluorescence change. In contrast, the folding kinetics at pH 5 is dominated by the fast phase, and the amplitude of the intermediate phase is reduced to ~10%. The pH-dependent amplitude changes show titration behavior with an apparent p*K* of ~5.7, consistent with the protonation of a single histidine residue. The intermediate phase can also be suppressed by the addition of 200 mM imidazole. Since both of these conditions interfere with histidine ligation, the intermediate kinetic phase is attributed to the presence of a non-native histidine ligand (His 26 or His 33) that can become trapped in a partially folded intermediate. In order to investigate the formation of H-bonded structure without interference from heme ligation events, quenched-flow and two-dimensional NMR methods were used to measure the time course of protection against NH exchange during the folding reaction at pH 5. In contrast to earlier results at higher pH, all amide protons had already acquired extensive protection during the fast folding phase, indicating a more cooperative structural transition. All except the N- and C-terminal amide protons exhibit a minor protection phase on the 100-ms time scale, suggesting that some preferential interaction of N- and C-terminal helices is also found at lower pH. A kinetic mechanism is presented that accounts for most of the observed structural and kinetic data on the cytochrome *c* folding process under various conditions. The model predicts that distinct populations of unfolded molecules with alternative axial ligands give rise to multiple parallel folding pathways, as previously observed [Elöve, G. A., & Roder, H. (1991) *ACS Symp. Ser. 470,* 50].

The structure, function, and folding of cytochrome *c* are intimately linked with the presence of a covalently attached ferrous or ferric heme group with axial ligands provided by the side chains of His 18 and Met 80 (Figure 1). The observation that apocytochrome *c* does not readily assume a stable folded structure in aqueous solution (Stellwagen et al., 1972; Fisher et al., 1973; Damaschun et al., 1991; Hamada et al., 1993) indicates that the native structure relies on stabilizing interactions of the polypeptide chain with the heme group. It has been shown by optical and NMR spectroscopy that one of the axial ligands in horse cyt *c*,[1] His 18, remains bound to the oxidized heme iron under typical denaturing conditions, such as in concentrated GuHCl or a urea solution near pH 7 (Babul & Stellwagen, 1971, 1972; Tsong, 1975; Muthukrishnan & Nall, 1991). On the other hand, the second axial ligand, Met 80, dissociates more readily even under mildly denaturing conditions, including pH values below 3 or above 9 (Greenwood & Palmer, 1965; Davis et al., 1974; Dyson & Beattie, 1982). The Met 80 ligand of native oxidized cyt *c* can also be displaced by the addition of extrinsic ligands, such as imidazole, azide, or cyanide (Babul & Stellwagen, 1971, 1972). In concentrated GuHCl or urea at neutral pH, the Met 80 ligand is replaced by a histidine side chain (Babul

† This work was supported by grants from the NIH (GM 35926 and CA06927), the NSF (MCB-9306367), and an appropriation from the Commonwealth of Pennsylvania to the Institute for Cancer Research.

* Correspondence should be addressed to this author at the Institute for Cancer Research, Fox Chase Cancer Center.

‡ Fox Chase Cancer Center.

§ University of Pennsylvania.

® Abstract published in *Advance ACS Abstracts,* May 15, 1994.

[1] Abbreviations: cyt *c*, horse heart cytochrome *c*; GuHCl, guanidine hydrochloride; pD, pH meter reading in D_2O; CD, circular dichroism.

0006-2960/94/0433-6925$04.50/0

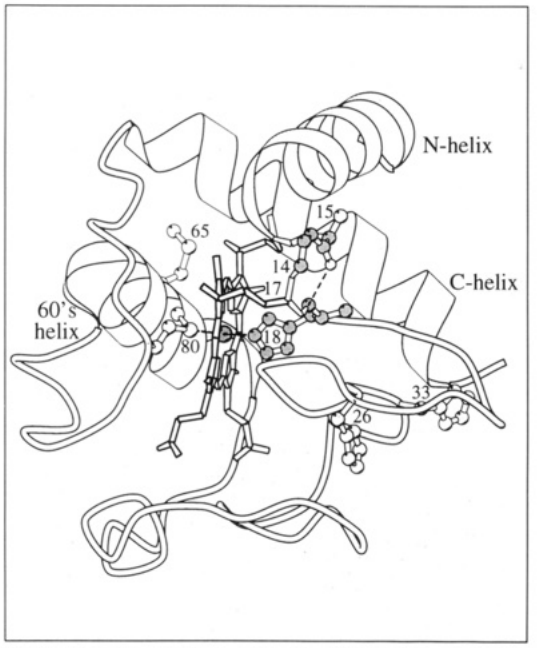

FIGURE 1: Structure diagram of horse cytochrome *c* based on the crystal structure (Bushnell et al., 1990). The ribbon diagram of the backbone conformation highlights the three main α-helical segments. The heme and its ligands, as well as potential non-native ligands (His 26, His 33, and Met 65), are shown explicitly. This figure was prepared with the program Molscript (Kraulis, 1991).

& Stellwagen, 1971; Muthukrishnan & Nall, 1991). In addition to His 18, horse cytochrome *c* has histidines at positions 26 and 33 that can share the sixth iron coordination site, along with other potential non-native ligands, such as Met 65 (Figure 1). Jones et al. (1993) recently applied laser photolysis and transient absorbance methods to investigate the dynamics of exchange among alternative heme ligands in reduced horse cyt *c* under denaturing conditions, as well as during the early stages of refolding.

A wealth of kinetic data on the folding process of oxidized horse cyt *c* revealed a complex interplay between conformational transitions, heme ligation events, and cis/trans isomerization of proline peptide bonds. These kinetic studies made use of a large number of conformational probes, including the following: the fluorescence of a single tryptophan, Trp 59, which becomes quenched during folding through energy transfer with the heme (Tsong, 1976; Brems & Stellwagen, 1983); changes in the heme absorption spectrum (Ikai et al., 1973; Brems & Stellwagen, 1983), which are dominated by the oxidation, ligation, and spin states of the heme iron; the far-UV and near-UV regions of the CD spectrum, which report on secondary structure formation and the burial of aromatic side chains, respectively (Elöve et al., 1992; Kuwajima et al., 1987); and finally, the protection of individual amide protons by hydrogen-bond formation during folding (Roder et al., 1988; Elöve & Roder, 1991) measured by quenched-flow hydrogen exchange in conjunction with two-dimensional NMR analysis (pulsed NH exchange). The time course of folding under strongly native conditions (i.e., low denaturant concentration, low temperature, and neutral pH) can be divided into four stages: a burst phase (<2 ms), a fast phase (2–100 ms), an intermediate phase (100 ms to 1 s), and a slow phase (>1 s). On the basis of changes in the far-UV CD spectrum, tryptophan fluorescence, and amide protection during the first few milliseconds of refolding, Elöve et al. (1992) concluded that a partially condensed state with fluctuating helical secondary structure is formed during the burst phase. The fast phase was first reported by Tsong (1973), who observed a minor process (15%) in pH-induced refolding experiments (jumping from pH 2 to 4) monitored by Soret absorbance. This process is accompanied by a substantial decrease in tryptophan fluorescence (Brems & Stellwagen, 1983; Roder et al., 1988), indicating that it corresponds to a major conformational step. Pulsed NH exchange studies showed that the only amide protons protected during the fast phase were located in two helical segments near opposite ends of the polypeptide chain: the N-helix (residues 3–14) and the C-helix (residues 87–103). Subsequent pulse labeling experiments at variable pH (Elöve & Roder, 1991) and the design of a peptide model (Wu et al., 1993) confirmed that this early folding intermediate contains a subdomain with the N- and C-terminal α-helices interacting through extensive hydrophobic contacts similar to those found in the native structure (Bushnell et al., 1990). The intermediate phase is characterized by major heme absorbance changes and further fluorescence quenching (Brems & Stellwagen, 1983). An increase in protection after $\sim$100 ms for amide probes in the 60's helix and in other nonregular regions indicates the formation of nativelike hydrogen-bonded structure (Roder et al., 1988). On the basis of the observation that the intermediate phase can be suppressed by adding imidazole or by lowering the pH, Brems and Stellwagen (1983) concluded that the ligation of Met 80 occurs during the intermediate phase [see also Myer (1984)], which was further supported by kinetic studies on iron-free cyt *c* (Henkens & Turner, 1979), as well as fragment recombination studies (Fisher & Taniuchi, 1992). Finally, most experimental parameters detect a minor slow phase (10–20%), which was shown to be caused by a slowly refolding subpopulation of unfolded molecules containing non-native cis peptide bonds at one or more proline residues [Ridge et al., 1981; see also Ramdas and Nall (1986)].

Although such a sequential folding process can account for most experimental observations, there are indications that the actual mechanism is even more complex. Pulsed NH exchange experiments under variable labeling conditions have shown that cyt *c* folding occurs along multiple parallel pathways (Elöve & Roder, 1991). This heterogeneous folding mechanism can be attributed to distinct populations of unfolded molecules with alternative heme ligands. Aiming toward a comprehensive structural and kinetic description of cyt *c* folding, we further investigated the ligand exchange processes in the denatured state and their coupling with conformational steps during folding. Kinetic folding studies based on optical probes and the protection of over 30 individual amide protons are fully consistent with a folding mechanism in which non-native histidine ligands can become trapped in early folding intermediates, including the previously detected intermediate with interacting chain termini (Roder et al., 1988). The rate-limiting step for further folding is the dissociation of this incorrect histidine ligand, which occurs on the 100-ms time scale, followed by the rapid assembly of remaining parts of the structure along with coordination of the Met 80 sulfur to the heme iron. The accumulation of this intermediate is suppressed under conditions that disfavor the formation of non-native histidine ligands, including lower pH and added imidazole, resulting in a more cooperative folding process with a rate corresponding to the fast folding phase.

MATERIALS AND METHODS

Materials and Sample Preparation. Horse heart ferricytochrome *c* (Type VI from Sigma Chemical Co.) was used without further purification. GuHCl was ultrapure grade from ICN-Schwarz/Mann. All other chemicals were reagent

grade. GuHCl concentrations were determined by refractive index measurements (Pace, 1986) on a Reichert-Jung Mark II Abbe refractometer (Leica, Inc., New York). Protein concentrations were determined spectrophotometrically using an extinction coefficient of 1.06×10^5 at 409 nm (Babul & Stellwagen, 1972). Final pH was measured for manually mixed solutions, as well as for the waste solution at the end of the stopped-flow experiments. The pH values at different stages of the pulse labeling experiment were determined by manual mixing. For D_2O solutions, uncorrected pH meter readings are reported as pD. Unfolded protein solutions were equilibrated for a minimum of 1 h prior to measurements.

Hydrogen Exchange Labeling. Pulsed NH exchange experiments (Roder et al., 1988; Udgaonkar & Baldwin, 1988) were performed on a QFM-5 quenched flow module (Bio-Logic, Echirolles, France) at 10 °C, following published procedures (Briggs & Roder, 1992; Roder et al., 1988). Oxidized cyt *c* (6 mM) was unfolded in an unbuffered D_2O solution containing 4.2 M deuterated GuHCl adjusted to pD 5. Under these conditions, all backbone amide protons exchange rapidly with deuterons from the solvent. Refolding was initiated by 6-fold dilution of the denatured protein with refolding buffer (100 mM acetate in H_2O), adjusted to yield a final pH of 5.0. The resulting refolding conditions (0.7 M GuHCl, pH 5, 10 °C, 83% H_2O/17% D_2O) are well below the equilibrium unfolding transition for cyt *c* (see Results). For the refolding periods used (5 ms to 60 s), D–H exchange is negligible even for unprotected amide groups. The D–H exchange reaction was initiated by rapidly mixing the partially refolded protein solution with an equal volume of 100 mM glycine buffer in H_2O at pH 9.8, resulting in a jump to pH 9.5. The 32-ms labeling pulse was terminated by lowering the pH to 5.3 in a final 1:1 mixing step with quench buffer (300 mM citrate at pH 5.3, containing 50 mM ascorbate as a reducing agent). For the preparation of NMR samples, the refolded and reduced protein was washed at 4 °C with several volumes of D_2O buffer (50 mM phosphate and 10 mM ascorbate at pH 5.3) and concentrated to about 2 mM, using ultrafiltration (Millipore YM3 membranes). The samples were incubated for 1 h at 30 °C to exchange marginally protected amide protons.

NMR Spectroscopy. ^1H NMR spectra were recorded at 500 MHz on a Bruker AM-500 spectrometer. Magnitude COSY spectra (Aue et al., 1976; Nagayama et al., 1980) were acquired and analyzed as previously reported (Roder et al., 1988). After one- and two-dimensional spectra were recorded, each sample was titrated to pD 7.0 and incubated for 4 h at 50 °C. Under these conditions, the more rapidly exchanging amide protons become deuterated, leaving about six highly protected amide protons that are well resolved in the one-dimensional NMR spectrum.

Optically Detected Stopped-Flow Measurements. All optically detected kinetic folding experiments were performed on a PQ/SF-53 stopped-flow instrument (Hi-Tech, Salisbury, England) equipped with a Berger-type mixer and a $2 \times 2 \times 10\,mm^3$ flow cell. For tryptophan fluorescence measurements, a 75-W xenon lamp (On-Line Instrument Systems, Inc., Jefferson, GA) and a monochromator (Hi-Tech) were used for excitation at 281 nm (5-nm bandwidth) along the 10-mm axis of the flow cell. The fluorescence emission was measured in the 2-mm direction using a high-pass glass filter with a 320-nm cutoff. To assess possible mixing artifacts and heat effects caused by GuHCl dilution, control experiments were performed using 100 μM *N*-acetyltryptophanamide solutions in 4.5 M GuHCl. Dilution (6-fold) with pH 7 buffer showed less than 5% apparent mixing artifacts within the first 10 ms and no evidence for heat effects. For folding experiments monitored via heme absorbance, the light from a tungsten lamp (LS-10, Hi-Tech) was passed through the monochromator set to a 5-nm bandwidth, and absorbance changes in the Soret or visible bands of oxidized cyt *c* were measured in the 2-mm direction of the flow cell. Data acquisition and analysis followed previously reported methods (Elöve et al., 1992).

For kinetic folding studies on oxidized cyt *c* at variable final pH values and fixed final denaturant concentration (0.7–0.75 M GuHCl), the folding reaction was initiated by the 6-fold dilution of unfolded cyt *c* (240 μM for fluorescence and 100 μM for absorbance) in 4.2–4.5 M GuHCl (pH 6.2–7) with refolding buffer at 10 °C. For fluorescence measurements, the buffer compositions were 50 mM citrate/50 mM phosphate (pH 4–5) and 50 mM acetate/50 mM phosphate (pH 5–7). The buffers used for absorbance measurements were 100 mM acetate (pH 4–5.5), 100 mM phosphate (pH 5.5–7.5), and 100 mM Tris (pH 7.5–8.0). All buffers except Tris were prepared from sodium salts. Equilibrium fluorescence measurements were performed at 10 °C on an SLM Aminco-Bowman luminescence spectrometer.

Rapid pH jumps for absorbance measurements under denaturing conditions were induced by mixing 1 part oxidized cyt *c* (100 μM) in 4.5 M GuHCl (10 mM phosphate) at pH 7.6 with 5 parts buffer containing 4.3 M GuHCl at 10 °C. The buffers used were 100 mM acetate and 10 mM phosphate for a final pH of 4.9 and 100 mM phosphate for a final pH of 2.1.

RESULTS

Hydrogen Exchange in GuHCl-Denatured cyt c. Information on the heme ligation and polypeptide conformation of cyt *c* in concentrated denaturant solution is limited to optical spectroscopic observations. For further structural characterization of denatured cyt *c*, we used quenched-flow and NMR methods (Robertson & Baldwin, 1991; Roder, 1989) to measure hydrogen exchange rates for individual backbone amide protons under denaturing conditions. The deuterium–hydrogen exchange reaction was initiated in a quenched-flow apparatus at 10 °C by mixing oxidized cyt *c* in D_2O buffer containing 4.5 M GuHCl with a 5-fold volume of H_2O buffer at the same pH (7.2) and denaturant concentration. After variable reaction times, exchange was quenched by rapidly lowering the pH to 5.3 with simultaneous dilution of the denaturant to native conditions (1.12 M). The quenched, oxidized cyt *c* samples were concentrated and transferred into D_2O buffer for analysis by one-dimensional proton NMR. Several additional amide protons were resolved by recording a second spectrum after ascorbate reduction of each sample.

Exchange rates obtained by exponential least-squares analysis of the resonance intensities versus exchange time are listed in Table 1, along with the corresponding intrinsic exchange rates predicted from model peptide data (Bai et al., 1993). The observed exchange rates for the amide protons of Thr 19, Gly 37, Leu 64, and Leu 98 are similar to the predicted rates within a factor of 2. Such lack of protection against exchange has been observed for several other thermally or chemically denatured proteins (Roder et al., 1985; Robertson & Baldwin, 1991; Radford et al., 1992a) and indicates that these amide protons are not involved in persistent hydrogen-bonded structure in the denatured state (Englander & Kallenbach, 1984). In contrast, the rate measured for His 18, 0.25 s^{-1}, is about 140 times slower than the corresponding

Table 1: Hydrogen Exchange Rates in GuHCl-Denatured Cytochrome *c*

	k_{ex} (s^{-1})[a]	k_{int} (s^{-1})[b]	$P = k_{int}/k_{ex}$
H18	0.25	34	140.00
T19	19	18	0.95
G37	47	33	0.70
L64	8.3	6.3	0.76
L98	11.2	4.5	0.40

[a] Deuterium–hydrogen exchange rates at 10 °C for oxidized cytochrome *c* in 4.5 M GuHCl, 50 mM phosphate, and 50 mM glycine (pH 7.2). [b] Intrinsic exchange rates predicted according to Bai et al. (1993), corrected for the effect of GuHCl on exchange rates (2.5-fold increase) reported by Loftus et al. (1986).

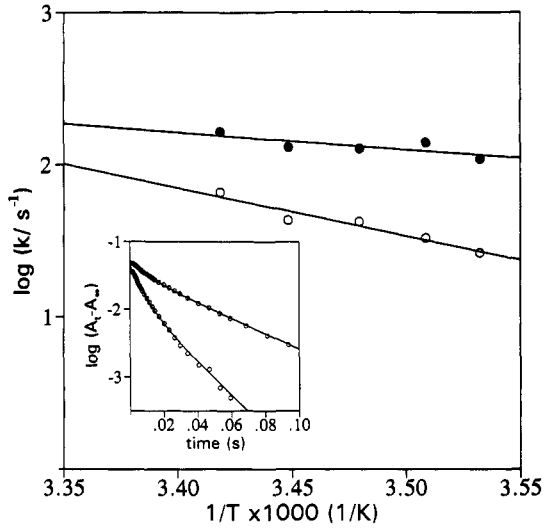

FIGURE 2: Kinetics of pH-dependent heme absorbance changes at 410 nm for oxidized cytochrome *c* in 4.5 M GuHCl measured by stopped-flow methods. The reaction was induced by a rapid jump from pH 7.8 to 4.6. The log of the rates of the two observed kinetic phases is plotted as a function of inverse absolute temperature. Relative errors (1 standard deviation) are ~8% for the faster rate and range between 4% (at 10 °C) and 10% (at 20 °C) for the slower rate. The activation energies are 5 ± 3 kcal/mol for the fast process and 14 ± 4 kcal/mol for the slow process. The inset shows the biphasic kinetic traces observed at 10 °C (top) and 20 °C (bottom).

intrinsic exchange rate of 34 s^{-1} calculated for a Cys-His dipeptide, according to Bai et al. (1993). For this calculation, we made the assumption that the rate for free uncharged His is also representative of iron-coordinated histidine, which is supported by the excellent agreement between observed and predicted rates for the adjacent Thr 19 NH. Protection factors in excess of 100 are generally observed only for hydrogen-bonded amide protons. Thus, the selective protection of the His 18 backbone NH provides strong evidence that it remains involved in a stable hydrogen-bonded interaction in the GuHCl-denatured state of cyt *c*.

Kinetics of pH-Dependent Spectral Changes in Denatured cyt c. The absorption difference spectrum between pH 7.5 and pH 5 solutions of GuHCl-denatured cyt c shows a pronounced maximum at 410 nm and a smaller minimum at 396 nm. In a series of stopped-flow experiments, we measured the time-dependent spectral changes at 410 nm for cyt c in 4.5 M GuHCl following a rapid jump from pH 7.8 to 4.6 at several temperatures in the range 10–20 °C (Figure 2). A satisfactory fit of the observed time course requires two exponentials, corresponding to a fast process with a rate of 110 s^{-1} at 10 °C and an apparent activation energy of 5 kcal/mol, and a slower process with a rate of 25 s^{-1} at 10 °C and an activation energy of 14 kcal/mol. Very similar kinetics was observed after a jump from pH 7.8 to 2.1, indicating that

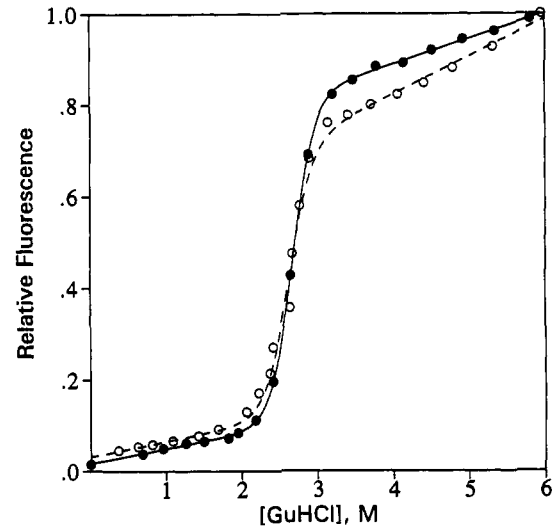

FIGURE 3: Fluorescence-detected GuHCl denaturation of oxidized cyt *c* at pH 5.0 (○, - - -) and pH 7.0 (●, —) and 10 °C. The curves were calculated by nonlinear least-squares analysis on the basis of a two-state model with a linear dependence of unfolding free energy ΔG on denaturant concentration: $\Delta G = \Delta G(0) - mC = m(C_m - C)$, with midpoints C_m = 2.67 ± 0.05 at pH 7.0 and C_m = 2.59 ± 0.07 M at pH 5.0, and a slope m = 3.9 ± 0.6 kcal mol^{-1} M^{-1} at both pH values.

the rate-limiting step is not a protonation event. Tsong (1975) previously observed a process similar to the slower phase following a jump from pH 10.5 to 5.2 for cyt *c* in 9 M urea, in addition to two slower processes not observed under our conditions.

Unfolding Equilibrium of cyt c. In order to find suitable unfolding and refolding conditions for subsequent kinetic studies, we measured the GuHCl-induced unfolding transition of cyt *c* at pH 5.0 and 7.0 (10 °C), using tryptophan fluorescence (Figure 3). The midpoint C_m = 2.67 ± 0.05 M and slope m = 3.9 ± 0.5 kcal mol^{-1} M^{-1} observed at pH 7.0 are similar to published values at higher temperatures (Tsong, 1974; Knapp & Pace, 1974). At pH 5, the unfolding transition was shifted to slightly lower GuHCl concentrations (C_m = 2.59 ± 0.07 M), and the slope (m = 3.9 ± 0.6 kcal mol^{-1} M^{-1}) remained, within error, unchanged. The more pronounced GuHCl-dependent increase in fluorescence in the baseline above the cooperative unfolding transition at pH 5, compared to pH 7, may be related to the dissociation of histidine ligands, which would allow the polypeptide chain to expand more freely with increasing denaturant concentration, or it may be due to pH-dependent changes in quenching efficiency. It should be noted that the fluorescence data in Figure 3 have been arbitrarily normalized relative to the value in 6 M GuHCl, since the effect of pH on the Soret spectrum and the resulting changes in quenching efficiency make the comparison of absolute fluorescence at pH 5 and 7 difficult.

Effect of Initial and Final pH on Optically Monitored Folding Kinetics. For optically detected stopped-flow measurements, the folding reaction of oxidized cyt *c* was triggered by a rapid jump in the GuHCl concentration from well above the unfolding transition (4.2–4.5 M) to concentrations well below (0.7–0.75 M), and the resulting fluorescence or absorbance changes were recorded at 10 °C over a time scale from about 2 ms to 1 min. Representative kinetic traces for different combinations of initial and final pH are shown in Figure 4, and the corresponding kinetic parameters are listed in Table 2.

As reported previously (Roder et al., 1988; Elöve et al., 1992), the fluorescence-detected folding kinetics at near-

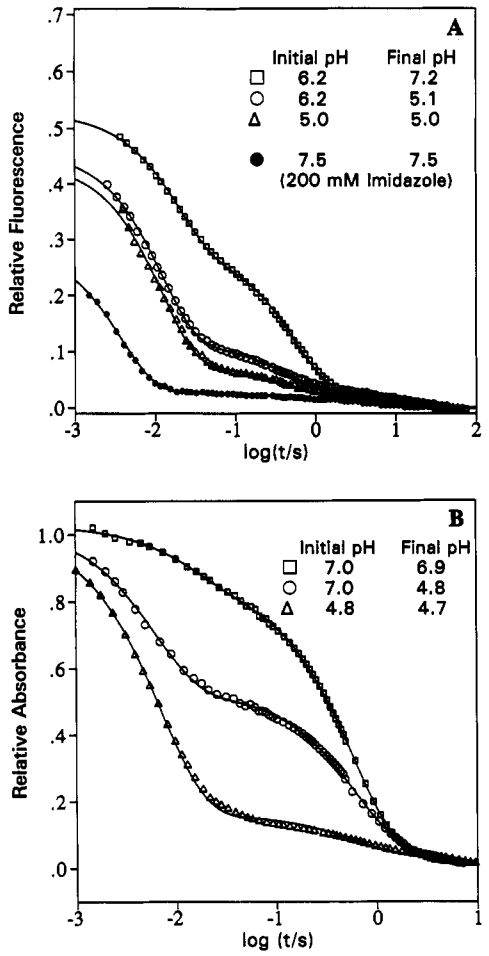

FIGURE 4: Representative stopped-flow traces for the refolding of GuHCl-denatured, oxidized cyt *c* at various initial and final pH values (10 °C) plotted on a logarithmic time scale. Panel A: Folding kinetics induced by GuHCl dilution from 4.2 to 0.7 M, monitored by tryptophan fluorescence (>310 nm). The bottom curve (●) shows the effect of imidazole on the folding kinetics, measured by fluorescence at 10 °C and pH 7.5, following a GuHCl concentration jump from 4.3 to 0.72 M in the presence of 200 mM imidazole. In each case, the fluorescence was normalized relative to the signal for the unfolded protein in 4.5 M GuHCl. Panel B: Folding kinetics induced by GuHCl dilution from 4.5 to 0.75 M monitored by heme absorbance at 410 nm. The curves represent nonlinear least-squares fits of three exponential phases. Absorbance data were normalized internally.

neutral pH (Figure 4A) exhibits four distinct processes: a very rapid decrease in fluorescence during the dead-time of the measurement (burst phase), a fast phase with a rate of ~50 s^{-1}, an intermediate phase with a rate of ~2 s^{-1}, and a minor slow phase with a rate of ~0.1 s^{-1}. Upon lowering the initial and final pH values to 5, we still observe three exponential processes with similar rates (Table 2), but the amplitude of the fast phase increases from 47% to 82% of the total observed fluorescence change (not counting the burst phase) at the expense of the intermediate-phase amplitude, which decreases from 47% to 12%. The burst-phase amplitude also increases toward lower pH (Figure 4A), but it is difficult to quantify this effect because of the pH-dependent changes in fluorescence quenching mentioned above.

The Soret absorbance changes at pH 7 (initial and final) shown in Figure 4B also display three kinetic phases, with rates similar to the fast, intermediate, and slow phases detected by fluorescence (no attempt was made to quantify any absorbance changes during the dead-time of the stopped-flow measurement). However, the two spectroscopic probes differ substantially in terms of relative amplitudes. The absorbance-detected kinetics is dominated by the intermediate phase, which accounts for 78% of the total change observed over a time window from 2 ms to 5 s, while the fast phase accounts for only about 15% of the absorbance change. This is in contrast to the fluorescence data, where both phases have similar amplitudes (Table 2). This effect is not due to the difference in initial pH, since we found very little change in the fluorescence-detected folding kinetics when the initial pH was increased from 6.2 to 7 (Table 2).

For many proteins, the kinetics of folding has been shown to be independent of the initial conditions used to unfold the protein (Creighton, 1988, 1990). However, we found that the folding kinetics of cyt *c* varies significantly as a function of initial pH. This effect is especially striking in Figure 4B, which compares the absorbance-detected folding kinetics at a final pH of 4.8 (in 0.75 M GuHCl) for initial pH values of either 7.0 or 4.8 prior to refolding (in 4.5 M GuHCl). When the initial pH is lowered from 7.0 to 4.8, the fractional amplitude of the intermediate phase decreases from 44% to 10% (Table 2), whereas the observed rates show much less variation. In the fluorescence-detected experiment (Figure 4A), the intermediate phase is less pronounced at high initial pH and decreases further when the initial pH is lowered from above 6 to about 5.

In a series of fluorescence-detected stopped-flow experiments (Figure 5), oxidized cyt *c* was unfolded in 4.2 M GuHCl at a constant pH of 6.2, and the pH of the refolding mixture was systematically varied over the range 4.1–7.3. The rates of the three kinetic phases show little variation with pH (Figure 5A). The increase in the relative amplitudes of the fast phase

Table 2: Observed Rates and Relative Amplitudes for Cytochrome *c* Folding as a Function of Initial and Final pH[a]

	phase					
	fast		intermediate		slow[b]	
	k_1 (s^{-1})	A_1	k_2 (s^{-1})	A_2	k_3 (s^{-1})	A_3
			Fluorescence			
pH 6.8 → 7.2	52 (1)	0.47 (0.004)	1.9 (0.03)	0.47 (0.003)	0.11 (0.01)	0.06 (0.003)
pH 6.2 → 5.1	84 (1)	0.75 (0.004)	2.7 (0.1)	0.17 (0.002)	0.08 (0.01)	0.08 (0.002)
pH 7.0 → 4.9	89 (2)	0.77 (0.006)	3.0 (0.2)	0.15 (0.004)	0.09 (0.01)	0.08 (0.004)
pH 5.0 → 5.0	84 (2)	0.82 (0.009)	2.6 (0.2)	0.12 (0.005)	0.06 (0.02)	0.06 (0.005)
			Heme Absorbance			
pH 7.0 → 6.9	68 (2)	0.17 (0.003)	1.8 (0.03)	0.78 (0.02)	0.14 (0.26)	0.05 (0.04)
pH 7.0 → 4.8	160 (4)	0.48 (0.006)	1.7 (0.07)	0.44 (0.02)	0.20 (0.20)	0.08 (0.01)
pH 4.8 → 4.7	139 (2)	0.84 (0.005)	2.5 (1.5)	0.10 (0.05)	0.15 (0.10)	0.06 (0.03)

[a] Rates (inverse of relaxation times) and relative amplitudes measured by stopped-flow methods at 10 °C. The final GuHCl concentration was 0.7 M for fluorescence-detected experiments and 0.75 M for heme-absorbance-detected experiments. The errors in individual parameters are indicated in parentheses (1 standard deviation). [b] The slow phase is not well defined in absorbance measurements because of convection artifacts.

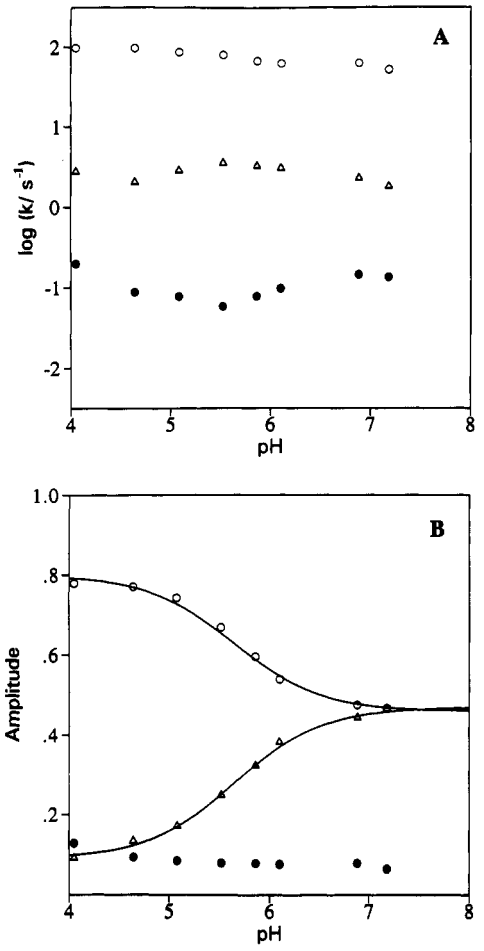

FIGURE 5: Fluorescence-detected folding kinetics of oxidized cyt *c* at 10 °C and 0.7 M GuHCl as a function of final pH. The protein was unfolded in 4.2 M GuHCl at pH 6.2. Panel A shows a log *k* versus pH plot for the fast (○), intermediate (△), and slow (●) kinetic phases. Panel B shows the dependence of the corresponding amplitudes (internally normalized), using the same symbols. Both solid lines show a one-proton titration curve for a transition with a p*K* of 5.7.

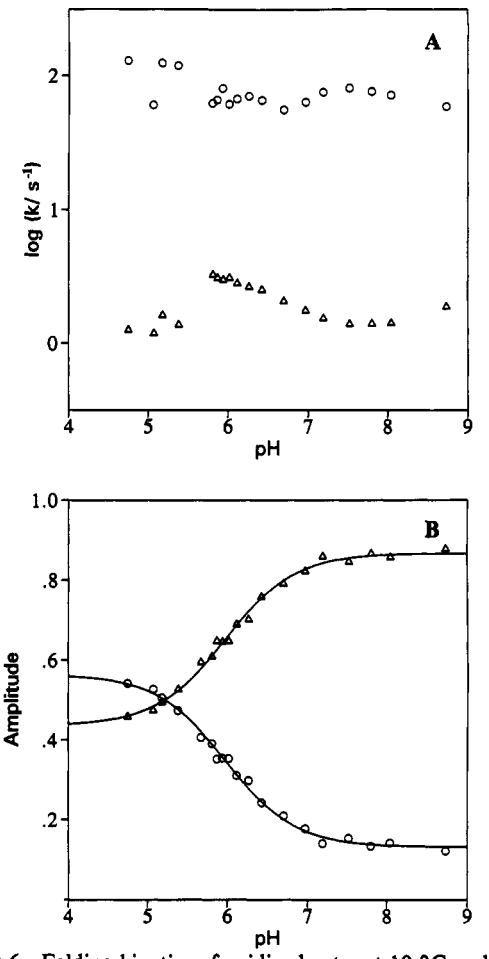

FIGURE 6: Folding kinetics of oxidized cyt *c* at 10 °C and 0.75 M GuHCl, monitored by Soret absorbance as a function of final pH. The protein was unfolded in 4.5 M GuHCl at pH 6.8. As in Figure 5, panel A shows a log *k* versus pH plot for the fast (○) and intermediate (△) phases, and panel B shows the corresponding internally normalized amplitudes (a minor slow phase was not well defined in this study). The solid lines represent titration curves for a transition with a p*K* of 5.9.

below pH 7 follows a one-proton titration curve with an apparent p*K* of 5.7 (Figure 5B). The pH dependence of the absorbance-detected folding kinetics shown in Figure 6 was measured under similar conditions (refolding from 4.5 M GuHCl at pH 6.8 to 0.75 M GuHCl at variable pH from 4.2 to 8.8). In this case, the increase in the fast-phase amplitude from 15% at pH 8 to 50% at pH 5 describes a titration curve with an apparent p*K* of 5.9. The close agreement of the p*K* values observed by fluorescence and by absorbance suggests that a single ionizing group, probably a histidine, is responsible for this transition. The somewhat lower p*K* value compared to that of a free imidazole group is consistent with the presence of a stabilizing interaction involving the neutral form of the histidine.

Effect of Imidazole on Fluorescence-Detected Folding Kinetics. Imidazole is known to bind to oxidized cyt *c*, both in the native state, where it replaces Met 80 as an axial heme ligand, and under denaturing conditions, where it displaces any weakly bound intrinsic ligand (Babul & Stellwagen, 1971; Muthukrishnan & Nall, 1991). Thus, imidazole binding is a useful approach for investigating the role of heme ligation in cyt *c* folding (Brems & Stellwagen, 1983; Myer, 1984). The presence of 200 mM imidazole prior to and during refolding has a dramatic effect on the folding kinetics of cyt *c* at neutral pH, as demonstrated by the fluorescence-detected stopped-flow results included in Figure 4A. In particular, the intermediate phase is completely eliminated by the addition of imidazole, as found in previous heme absorbance measurements (Brems & Stellwagen, 1983). In addition, we observed a 5-fold increase in the rate of the fast phase and a major increase in the burst-phase amplitude.

Folding Kinetics of cyt c at pH 5 Studied by Pulsed NH Exchange. In previous pulsed NH exchange studies, we measured the protection of amide protons against D–H exchange during the refolding of oxidized cyt *c* at pH 6.2 (Roder et al., 1988). The results presented above suggest that, under these conditions, the folding process may be complicated by the presence of non-native histidine ligands. Therefore, we decided to repeat these experiments at a refolding pH of 5, where interference from non-native heme ligands is less likely. All other experimental conditions were chosen to match our previous folding experiments (Roder et al., 1988; Elöve et al., 1992). The time course of protection at pH 5 is illustrated in Figure 7 for a representative set of amide protons from various regions of the protein. The observed decrease in proton occupancy toward longer folding times reflects the increasing level of protection of individual ND groups against exchange with solvent protons as they become involved in stable hydrogen-bonded interactions during folding. Under our labeling conditions (pH 9.5, 10 °C), exchange time constants in the range 0.2–5 ms are predicted from model peptide data (Bai et al., 1993). Thus, unprotected NH groups are protonated within the first 5 ms of the labeling

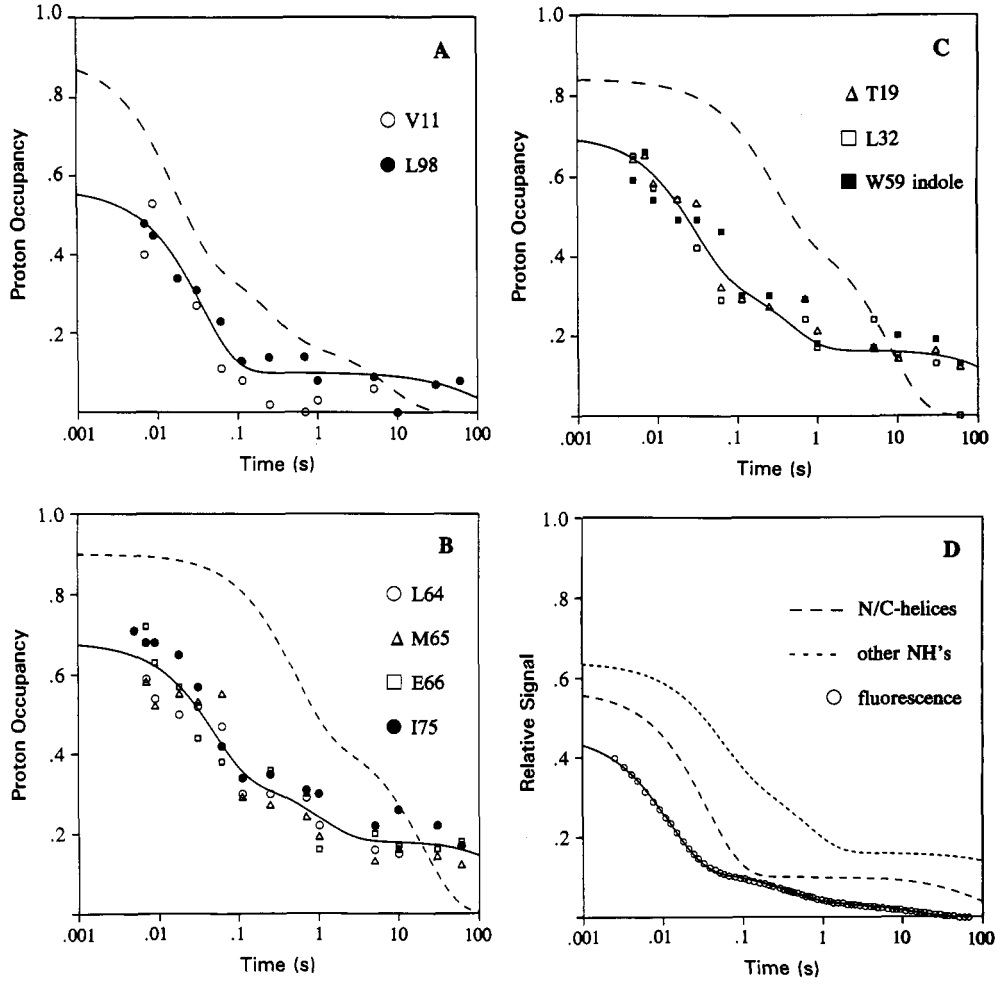

FIGURE 7: Time course of protection from D–H exchange for representative backbone and side-chain amide sites during the refolding of oxidized cyt *c* at pH 5 and 10 °C. Proton occupancy is plotted versus refolding time on a logarithmic scale (1 ms to 100 s). Solid curves indicate approximate two- or three-exponential fits, and broken curves represent the corresponding fits obtained in a previous study at a refolding pH of 6.2 (Roder et al., 1988). Panel A shows representative NH probes in the N- and C- terminal helices, and panel B shows examples from the 60's and 70's helices. Two main-chain and one side-chain NH involved in tertiary hydrogen bonds are shown in panel C. Panel D shows a comparison of the fluorescence-detected stopped-flow kinetics at pH 5 with the time course of protection for the two classes of amide protons observed by pulsed NH exchange under the same folding conditions.

pulse, which makes it possible to resolve kinetic processes on a much shorter time scale than the duration of the labeling pulse (32 ms).

Compared to the previous data at higher refolding pH, we observed significantly lower proton occupancies at all except the longest folding times, which is primarily due to a higher level of protection during the 5-ms dead-time of the quenched-flow experiment. Most amide protons become 35–50% protected during the first 5 ms of refolding, in contrast to the previous data, which showed at most 20% protection during the dead-time. By comparing the observed time course of protection for different protons at pH 5 (Figure 7D), we can distinguish two groups of amide protons with distinct kinetic behavior. The first group includes Val 11 and Leu 98 (Figure 7A), as well as 14 other amide protons in the N- and C-terminal α-helices, which undergo extensive protection (>40%) during the dead-time, followed by another 50% increase in protection during a fast phase (30–60 s^{-1}) and a minor slow phase (<0.1 s^{-1}) with less than 10% amplitude. All other amide protons exhibit an additional intermediate phase with a rate of 1–2 s^{-1} and an amplitude of about 20%. Amide protons in this second group show less protection during the dead-time (20–35%) and a fast phase with reduced amplitude (~40%), while the slow phase is more pronounced (15–25%). Two amide protons in the short 70's helix, Tyr 74 and Ile 75, show similar kinetic features with somewhat higher occupancies over the entire time window (Figure 7B).

Lowering the pH of refolding from 6.2 (dashed lines in Figure 7) to 5 (solid lines) results in pronounced kinetic changes. At pH 6.2, the only amides protected on the 10-ms time scale (fast phase) were those at the interface between the N- and C-terminal helices (Roder et al., 1988; Figure 7A), while all other amide probes remained largely unprotected out to about 100 ms (Figure 7B,C). In contrast, at pH 5, all protons experience a significant increase in protection on the time scale of the fast phase (15–30 ms), whereas the intermediate phase is either absent (for N- and C-terminal amides) or strongly reduced in amplitude (all other NH probes). The effect of pH on the early stages of cyt *c* folding is illustrated in Figure 8, which compares the protection patterns at pH 5 and 6.2 at a common refolding time of 30 ms. The preferential protection of N- and C-terminal amide protons seen at pH 6.2 is less pronounced at pH 5. For example, at pH 6.2 the average occupancy in the two terminal α-helices is about 0.5, which is substantially lower than that for the 60's helix (~0.85), in contrast to pH 5 where the average occupancy of N- and C-terminal amide protons (~0.3) is only slightly lower than that for the 60's helix (~0.4).

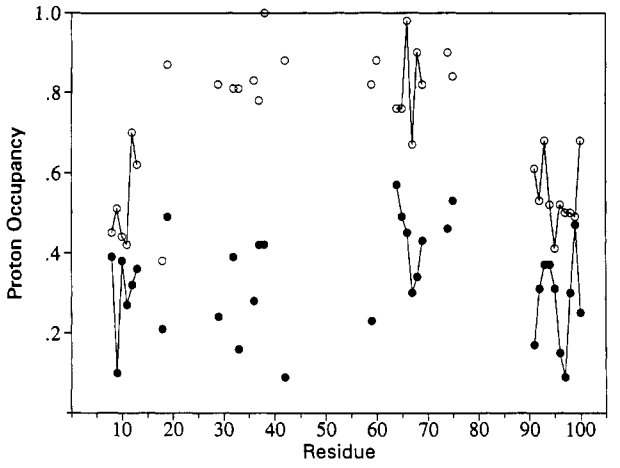

FIGURE 8: Comparison of NH protection patterns measured by pulse labeling at a refolding time of 30 ms during cyt *c* folding at pH 5 (●) and pH 6.2 (○).

DISCUSSION

Heme Ligation and Residual Structure in GuHCl-Denatured cyt c. The heme absorption spectrum of cyt *c* provides qualitative information on the number and identity of axial ligands to the heme iron under various native and denaturing conditions (Margoliash & Schejter, 1966; Babul & Stellwagen, 1971, 1972; Tsong, 1975; Dyson & Beattie, 1982; Brems & Stellwagen, 1983). Guanidine- or urea-denatured, oxidized cyt *c* at neutral pH exhibits a Soret maximum at 406 nm and no 620-nm band, which is characteristic of a low-spin form with two strong-field axial ligands. Because of the covalent attachment of the heme to Cys 14 and Cys 17, His 18 is very likely to be one of these ligands. However, the 695-nm band, a unique marker for the presence of an iron–sulfur bond (Schechter & Saludjian, 1967; Schejter et al., 1991), is no longer observed, indicating that the native Met 80 ligand is displaced by another side chain. Muthukrishnan and Nall (1991) recently confirmed previous indications (Babul & Stellwagen, 1971; Elöve & Roder, 1991) that this non-native ligand is a histidine. Using proton NMR to analyze cytochromes c from various species, they concluded that the conserved His 18 remains bound in the GuHCl-unfolded state, whereas other histidines (His 26 and His 33 in the case of horse cyt *c*) compete for the sixth iron binding site. The only additional side chain that could potentially serve as a heme ligand at near-netural pH is Met 65, but this is unlikely, considering the absence of the 695-nm band and the fact that methionine analogues bind only very weakly to oxidized model hemes (Harbury et al., 1965).

Our hydrogen exchange evidence for H-bonded residual structure involving the main chain of His 18 provides further support for the ligation of the His 18 side chain to the heme in unfolded cyt *c*. In the native structure (Bushnell et al., 1990), the backbone NH of His 18 forms a hydrogen bond with the carbonyl of Ala 15. Given the adjacent covalent attachment of the heme via Cys 14 and Cys 17, it is reasonable to conclude that this H-bond remains intact under denaturing conditions that favor the ligation of His 18 to the heme iron.

Histidine ligands are expected to dissociate at low pH, since protonation of the histidine Nδ is incompatible with heme ligation. Indeed, acidification of cyt *c* in 9 M urea results in a shift of the Soret band from 406 to 395 nm and the appearance of a new absorption band at 620 nm with an apparent p*K* value of 5.2, suggesting the formation of a high-spin complex in which the strong-field histidine ligands have been replaced by weak-field ligands from the solvent (Babul & Stellwagen, 1971). Acid titration in 6 M GuHCl shows a similar transition with a p*K* of 5.1 (Tsong, 1975). However, compared to urea, the Soret band of the acidic form (below pH 4.5) is less intense and lies at higher wavelength (398 nm), suggesting partial binding of an axial ligand perhaps due to the high ionic strength of the GuHCl solution, which favors compact conformations (Goto et al., 1993). The presence of one or two His ligands in unfolded cyt *c* is consistent with the spectral properties of heme-containing fragments of cyt *c*. At neutral pH, the Soret maximum for heme fragment 1–38, which includes all three histidine residues of horse cyt *c*, is identical to that of the whole protein in denaturant (406 nm), in contrast to heme fragment 14–21 lacking His 26 and His 33, which shows a partially blue-shifted Soret band at 398 nm even at neutral pH (Babul & Stellwagen, 1971). The only available ligand in this fragment, His 18, is dissociated with an apparent p*K* of 3.8, producing the characteristic high-spin spectrum with a Soret maximum at 394 nm (Babul & Stellwagen, 1972).

Dynamics of Ligand Exchange in Unfolded cyt c. The relaxation processes observed by heme absorbance measurements following acidification of GuHCl-denatured cyt *c* can be attributed to the dissociation of the non-native histidine ligand from the heme iron, followed by rapid protonation of the free histidine side chain. In preliminary experiments on a mutant form of horse cyt *c* containing a His to Gln substitution at residue 26, we observed a single exponential phase with a rate of 36 s^{-1} (unpublished results). Therefore, we tentatively interpret the two kinetic phases observed for the wild-type protein as the dissociations of His 26 (110 s^{-1}) and His 33 (25 s^{-1}), respectively. In recent nanosecond laser photolysis studies, Jones et al. (1993) observed analogous intramolecular ligation events in the unfolded state of reduced cyt *c*, following the photodissociation of a carbon monoxide ligand. They showed by kinetic modeling that transient binding and dissociation of histidine ligands occur on the 100-μs time scale, indicating that the dynamics of ligand binding and dissociation are much faster in the reduced state of the heme.

Kinetic Mechanism of cyt c Folding. The dynamic equilibrium among various unfolded species differing in heme coordination is a key feature for understanding the folding mechanism of cyt *c*. Because of their relatively slow rate of dissociation, non-native histidine ligands can become trapped during refolding. As a working model, we propose the kinetic mechanism shown in Figure 9A. In this scheme, unfolded molecules (U) are assumed to retain His 18 as the fifth heme ligand, and different species are labeled according to the side chains that can serve as a possible sixth ligand, including His 26 (U^{H26}) and His 33 (U^{H33}), in addition to the native Met 80 (U^{M80}). U* represents 5-coordinate forms of the unfolded protein or species with a weak solvent ligand, and I* designates any folded or nativelike forms lacking an intramolecular sixth ligand. The existence of I* is not only physically plausible but also necessary to explain the unfolding kinetics of cyt *c* (manuscript in preparation). I^{H26} and I^{H33} identify partially folded intermediates with non-native histidine ligands. Finally, N^{M80} stands for the native form with the correct Met 80 ligand. Horizontal arrows indicate major conformational transitions accompanied by large fluorescence changes, whereas vertical arrows indicate changes in heme ligation accompanied by heme absorbance changes. The kinetic mechanism in Figure 9A does not account for the minor slow folding phases attributed to proline cis/trans isomerization [Ridge et al., 1981; see also Ramdas and Nall (1986) and Wood et al. (1988)

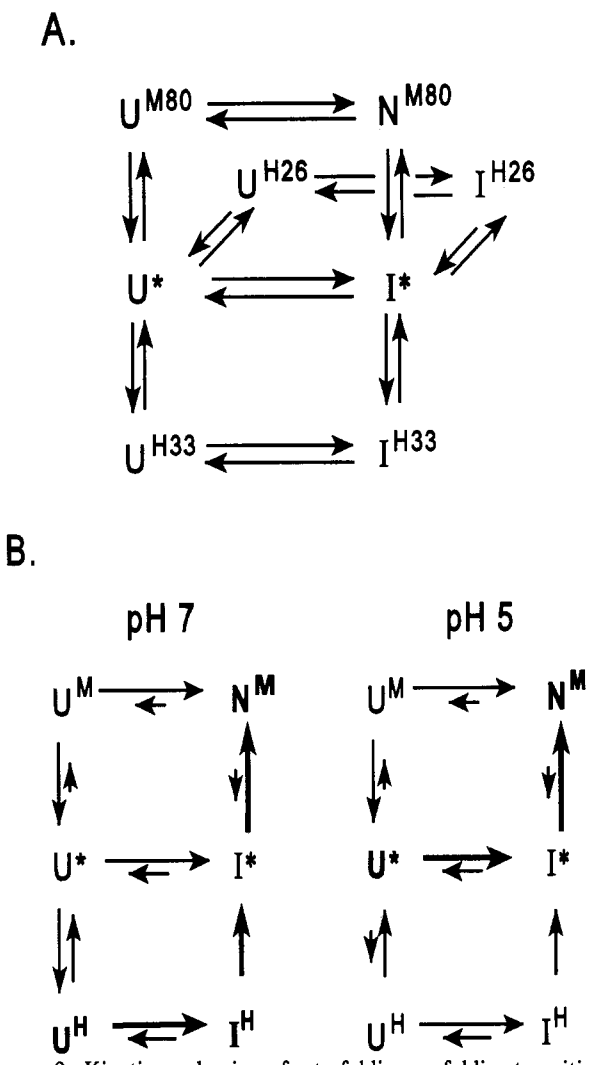

FIGURE 9: Kinetic mechanism of cyt *c* folding–unfolding transitions and their coupling with heme ligation. Panel A: N^{M80} and U^{M80} represent folded and unfolded states containing the native Met 80 ligand; U^{H26} and U^{H33} designate unfolded states with a non-native His 26 or His 33 ligand at the sixth iron coordination site; I^{H26} and I^{H33} are intermediates with trapped non-native ligands; I* and U* represent 5-coordinate folded and unfolded states, respectively. All forms contain His18 as the fifth ligand. Panel B: The predominant folding pathways at pH 7 (left) and pH 5 (right) are highlighted. Unfolded states with non-native His ligands, U^{H}, are populated above pH 6, and folding proceeds through partially folded intermediates I^{H}. Below pH 6 (right), the distribution of unfolded states shifts toward U*, and folding proceeds through a structured 5-coordinate state, I*, followed by rapid Met 80 ligation.

for results on the homologous yeast iso-2 cyt *c*]. The inclusion of states with non-native proline isomers would result in a much more complex scheme with dozens of states. The kinetic mechanism also does not fully account for very early folding events, including the burst-phase intermediate detected in previous kinetic circular dichroism and fluorescence studies (Elöve et al., 1992).

Optically Monitored Folding Kinetics at Neutral pH. The predominant unfolded species at equilibrium near pH 7 are U^{H26} and U^{H33}, and a significant fraction of the molecules begin to fold with an alternative ligand bound (since the two histidines play similar roles and cannot be distinguished at this time, we collectively identify unfolded and partially folded species with a non-native histidine ligand as U^{H} and I^{H}, respectively). Folding at neutral pH thus proceeds along the pathway, $U^{H} \rightarrow I^{H} \rightarrow I^{*} \rightarrow N^{M80}$, highlighted in Figure 9B. The fast folding phase (50 s^{-1}) corresponds to the $U^{H} \rightarrow I^{H}$ folding transition, and the intermediate phase (~2 s^{-1}) corresponds to the $I^{H} \rightarrow I^{*}$ step, i.e., the dissociation of a non-native histidine ligand in a partially folded state. The large decrease in fluorescence associated with the fast phase indicates that the fluorescence of Trp 59 is substantially quenched in the I^{H} intermediate, which is consistent with previous evidence for the compact nature of this state (Roder et al., 1988; Elöve et al., 1992). On the other hand, the small change in Soret absorbance that accompanies the fast phase confirms that no change in ligation occurs during the fast phase. It is interesting to note that the rate of dissociation for non-native histidine ligands under refolding conditions is at least 20 times slower than the corresponding rates under denaturing conditions, as expected for a ligand trapped in a partially folded state.

Effect of pH and Extrinsic Ligands. The folding mechanism shown in Figure 9 is fully consistent with the pH-dependent changes observed in folding kinetics. Lowering the pH from above 6 to about 5 shifts the equilibrium of unfolded species from U^{H} toward U*. This shift must be due to a decrease in the association rates ($U^{*} \rightarrow U^{H}$), since the dissociation rates for His 26 and His 33 were found to be pH-independent. The I^{H} intermediate is thus bypassed at pH 5, and the dominant folding pathway is $U^{*} \rightarrow I^{*} \rightarrow N^{M80}$, where the first step is the rate-limiting conformational change followed by rapid ligation of the Met 80 ligand. This mechanism explains the greatly diminished amplitude for the intermediate phase observed at low pH (Figures 4–6).

Our interpretation is further supported by the fact that the addition of imidazole selectively eliminates the intermediate folding phase (Figure 4A). By replacing any intramolecular ligand at the sixth iron coordination site with an extrinsic ligand, the kinetic mechanism is essentially reduced to the $U^{*} \leftrightarrow I^{*}$ transition (Figure 9). However, it is important to note that the folding reaction at high imidazole concentration does not proceed all the way to the native state, since the extrinsic ligand remains bound under native conditions (Babul & Stellwagen, 1971).

The formation of axial heme ligands can also be prevented by removal of the heme iron (Henkens & Turner, 1979), which results in a destabilized, but still folded, species (porphyrin *c*). Henkens and Turner (1979) reported that the optically monitored folding reaction of porphyrin *c* occurs in a single rapid kinetic phase with a rate of 70 s^{-1} (at 25 °C in 0.75 M GuHCl, pH 6.5), which is comparable to the fast folding phase of the holoprotein. The folding behavior of porphyrin *c* also resembles that of the imidazole complex, suggesting that the His 18 ligand, which is present only in the latter case, is not an essential requirement at the early stages of folding. The absence of an intermediate folding phase for porphyrin *c* again supports our conclusion that it is coupled with heme ligation events. However, a later conflicting report of a minor (18%) intermediate phase (175 ms) observed at pH 7 for porphyrin *c* (Brems & Stellwagen, 1983) is difficult to consolidate with our kinetic model. Given the weight of evidence for assigning the intermediate phase to an iron ligation event, we suspect that this puzzling result may be an experimental artifact, perhaps due to incomplete extraction of the heme iron or contamination with another metal.

The kinetic mechanism proposed in Figure 9 can also account for the unusual effect of initial pH on the folding kinetics at pH 5 (Figure 4). Since U^{H} is the predominant initial state above pH 6 (cf. Figure 5), one expects the partial accumulation of I^{H}, even if the pH is lowered to 5 during refolding, which explains the high intermediate-phase amplitude observed by

absorbance. However, it is more difficult to understand the corresponding fluorescence data, which showed little intermediate phase at pH 5, independent of the initial pH (5.0, 6.2, or 7.0). A possible explanation for this apparent discrepancy is that the fluorescence of Trp 59 in I^H becomes more completely quenched at lower pH.

Structural Mechanism of Folding. Our earlier pulsed NH exchange results at pH 6.2 (Roder et al., 1988) led to the conclusion that the N- and C-terminal α-helices of cyt *c* form and associate during the fast folding phase on the 10-ms time scale (cf. Figures 7 and 8). The resulting partially folded intermediate corresponds to the I^H state in our kinetic scheme (Figure 9B). Since His 26 and His 33 are far from the chain termini (Figure 1), their ligation to the heme iron does not interfere with the docking of the N- and C-terminal helices. On the other hand, the presence of non-native ligands is likely to prevent the formation of correctly folded structure in other parts of the molecule, including the loop region spanning residues 20–60, as well as the 60's and 70's helices that are in close contact with Met 80 in the native structure (Figure 1). The presence of a non-native heme ligand serves as a kinetic trap that leads to the accumulation of a long-lived intermediate and makes it experimentally observable. In this sense, the involvement of heme ligands in cyt *c* folding is analogous to that of proline or disulfide isomerization (noncovalent), as well as disulfide formation and exchange during the oxidative refolding of other proteins (Creighton, 1990; Weissman & Kim, 1991; Schmid, 1992).

On the basis of pulsed NH exchange experiments at variable labeling pH (Elöve & Roder, 1991), we concluded that the cyt *c* folding mechanism is heterogeneous, i.e., that the protein folds along several parallel pathways. Similar observations have been reported for other proteins (Radford et al., 1992b; Jennings et al., 1993; Roder & Elöve, 1994). One likely cause of heterogeneous folding behavior is the slow isomerization of proline peptide bonds in the unfolded state (see below). However, in the case of cyt *c*, parallel folding pathways can also arise from the existence of multiple unfolded states with alternative axial heme ligands undergoing exchange on a relatively slow time scale ($\sim$10 ms). Our kinetic mechanism predicts up to four parallel pathways under conditions where all four unfolded species are populated. For example, a small population ($\sim$15%) of Met 80-ligated unfolded molecules (U^{M80}) would explain a minor fraction of very rapidly protected molecules detected by pulsed NH exchange (Roder et al., 1988; Elöve & Roder, 1991). Some of the complexities in amide protection kinetics on the time scale of the intermediate phase may reflect differences in folding for molecules containing either His 26 or His 33 as a ligand. This mechanism can easily be extended by including other potential heme ligands, such as Met 65 or deprotonated lysine side chains (at high pH).

The optical results discussed above indicate that heme ligation and conformational events can be largely decoupled by lowering the pH. Indeed, our pulsed NH exchange study at pH 5 (Figure 7) reveals a more cooperative folding process in which all amide protons acquire at least partial protection during the fast folding phase, consistent with a more direct folding pathway ($U^* \rightarrow I^* \rightarrow N^{M80}$). Nevertheless, we observe multiple kinetic phases and interesting differences in the time course of protection among individual amide probes especially in the 100-ms time range, where all except N- and C-terminal amide protons exhibit a minor intermediate phase (Figure 7). One possible explanation for this residual intermediate phase is that one of the histidine ligands is still partially bound at pH 5; a likely candidate is His 33, which appears to dissociate more slowly than His 26. Another possibility is that this process reflects a different conformational event unrelated to heme ligation.

Other differences in protection patterns can be attributed to proline peptide bond isomerization, especially at long times, where N- and C-terminal amide protons show somewhat lower proton occupancies than other probes. It is possible that proline isomerization is coupled with heme ligation events. For example, the correct coordination of Met 80 to the iron might be possible only if the nearby prolines at positions 71 and 76 are in their native trans state, which might explain the slow folding phase observed by heme absorbance. Brems and Stellwagen (1983) suggested such a mechanism to explain the intermediate and slow phases in cyt *c* folding. However, the rate of the intermediate phase (2 s^{-1}) seems to be too fast for a proline isomerization step, even if one allows for a possible acceleration by structural constraints (Texter et al., 1992). Thus, we favor the mechanism shown in Figure 9, which provides a satisfactory explanation of the intermediate phase without invoking proline isomerization. It should be emphasized that the heme ligands are unlikely to play an active role in folding. Rather, they can serve as kinetic traps that allow structural intermediates to accumulate that would otherwise escape detection. In particular, the preferential interaction between helical segments near opposite ends of the chain can occur irrespective of the heme ligation state. This conclusion is supported by recent model peptide studies (Wu et al., 1993), which showed that a synthetic peptide corresponding to the C-terminal helix of cyt *c* can form a specific binary complex with a heme-containing N-terminal fragment, even in the absence of the intervening parts of the polypeptide chain.

ADDED IN PROOF

A related study on the kinetics of cytochrome *c* folding at low pH appeared after submission of this paper (Sosnick et al., 1994).

ACKNOWLEDGMENT

We are grateful to Drs. W. Colón and S. D. Luck for their help with experiments and many useful discussions. We also thank Dr. G. D. Markham for his critical reading of the manuscript and J. M. Sauder for his assistance with molecular graphics.

REFERENCES

Aue, W. P., Bartholdi, E., & Ernst, R. R. (1976) *J. Chem. Phys. 64*, 2229–2246.

Babul, J., & Stellwagen, E. (1971) *Biopolymers 10*, 2359–2361.

Babul, J., & Stellwagen, E. (1972) *Biochemistry 11*, 1195–1200.

Bai, Y., Milne, J. S., & Englander, S. W. (1993) *Proteins 17*, 75–86.

Brems, D. N., & Stellwagen, E. (1983) *J. Biol. Chem. 258*, 3655–3660.

Briggs, M. S., & Roder, H. (1992) *Proc. Natl. Acad. Sci. U.S.A. 89*, 2017–2021.

Bushnell, G. W., Louie, G. V., & Brayer, G. D. (1990) *J. Mol. Biol. 214*, 585–595.

Creighton, T. E. (1988) *Proc. Natl. Acad. Sci. U.S.A. 85*, 5082–5086.

Creighton, T. E. (1990) *Biochem. J. 270*, 1–16.

Damaschun, G., Damaschun, H., Gast, K., Gernat, C., & Zirwer, D. (1991) *Biochim. Biophys. Acta 1078*, 289–295.

Davis, L., Schejter, A., & Hess, G. P. (1974) *J. Biol. Chem. 249*, 2624–2632.

Dyson, H. J., & Beattie, J. K. (1982) *J. Biol. Chem. 257*, 2267–2273.
Elöve, G. A., & Roder, H. (1991) in *Protein Refolding* (Georgiou, G., Ed.) ACS Symposium Series No. 470, pp 50–63, American Chemical Society, Washington, D.C.
Elöve, G. A., Chaffotte, A. F., Roder, H., & Goldberg, M. E. (1992) *Biochemistry 31*, 6876–6883.
Englander, S. W., & Kallenbach, N. R. (1984) *Q. Rev. Biophys. 16*, 521–565.
Fisher, A., & Taniuchi, H. (1992) *Arch. Biochem. Biophys. 296*, 1–16.
Fisher, W. R., Taniuchi, H., & Anfinsen, C. B. (1973) *J. Biol. Chem. 248*, 3188–3195.
Goto, Y., Hagihara, Y., Hamada, D., Hoshino, M., & Nishii, I. (1993) *Biochemistry 32*, 11878–11885.
Greenwood, C., & Palmer, G. (1965) *J. Biol. Chem. 240*, 3660–3663.
Hamada, D., Hoshino, M., Kataoka, M., Fink, A. L., & Goto, Y. (1993) *Biochemistry 32*, 10351–10358.
Harbury, H. A., Cronin, J. R., Fanger, M. W., Hettinger, T. P., Murphy, A. J., Myer, Y. P., & Vinogradov, S. N. (1965) *Proc. Natl. Acad. Sci. U.S.A. 54*, 1658–1664.
Henkens, R. W., & Turner, S. R. (1979) *J. Biol. Chem. 254*, 8110–8112.
Ikai, A., Fish, W. W., & Tanford, C. (1973) *J. Mol. Biol. 73*, 165–184.
Jennings, P. A., Finn, B. E., Jones, B. E., & Matthews, C. R. (1993) *Biochemistry 32*, 3783–3789.
Jones, C. M., Henry, E. R., Hu, Y., Chan, C.-K., Luck, S. D., Bhuyan, A., Roder, H., Hofrichter, J., & Eaton, W. A. (1993) *Proc. Natl. Acad. U.S.A. 90*, 11860–11864.
Knapp, J. A., & Pace, C. N. (1974) *Biochemistry 13*, 1289–1294.
Kraulis, P. J. (1991) *J. Appl. Crystallogr. 24*, 946–950.
Kuwajima, K., Yamaya, H., Miwa, S., Sugai, S., & Nagamura, T. (1987) *FEBS Lett. 221*, 115–118.
Loftus, D., Gbenle, G. O., Kim, P. S., & Baldwin, R. L. (1986) *Biochemistry 25*, 1428–1436.
Margoliash, E., & Schejter, A. (1966) *Adv. Protein Chem. 21*, 113–286.
Muthukrishnan, K., & Nall, B. T. (1991) *Biochemistry 30*, 4706–4710.
Myer, Y. P. (1984) *J. Biol. Chem. 259*, 6127–6133.
Nagayama, K., Kumar, A., Wüthrich, K., & Ernst, R. R. (1980) *J. Magn. Reson. 40*, 321–334.
Pace, C. N. (1986) *Methods Enzymol. 131*, 266–280.
Radford, S. E., Buck, M., Topping, K., Dobson, C. M., & Evans, P. A. (1992a) *Proteins 14*, 237–248.
Radford, S. E., Dobson, C. M., & Evans, P. A. (1992b) *Nature 358*, 302–307.
Ramdas, L., & Nall, B. T. (1986) *Biochemistry 26*, 6959–6964.
Ridge, J. A., Baldwin, R. L., & Labhardt, A. M. (1981) *Biochemistry 20*, 1622–1630.
Robertson, A. D., & Baldwin, R. L. (1991) *Biochemistry 30*, 9907–9914.
Roder, H. (1989) *Methods Enzymol. 176*, 446–472.
Roder, H., & Elöve, G. A. (1994) in *Mechanisms of Protein Folding* (Pain, R. H., Ed.), pp 26–54, Oxford Univ. Press, New York.
Roder, H., Wagner, G., & Wüthrich, K. (1985) *Biochemistry 24*, 7407–7411.
Roder, H., Elöve, G. A., & Englander, S. W. (1988) *Nature 335*, 700–704.
Schechter, E., & Saludjian, P. (1967) *Biopolymers 5*, 788–790.
Schejter, A., Plotkin, B., & Vig, I. (1991) *FEBS Lett. 280*, 199–201.
Schmid, F. X. (1992) *Curr. Opin. Struct. Biol. 2*, 21–25.
Sosnick, T. R., Mayne, L., Hiller, R., & Englander, S. W. (1994) *Nature Struct. Biol. 1*, 149–156.
Stellwagen, E., Rysavy, R., & Babul, G. (1972) *J. Biol. Chem. 247*, 8074–8077.
Texter, F. L., Spencer, D. B., Rosenstein, R., & Matthews, C. R. (1992) *Biochemistry 31*, 5687–5691.
Tsong, T. Y. (1973) *Biochemistry 12*, 2209–2214.
Tsong, T. Y. (1975) *Biochemistry 14*, 1542–1547.
Tsong, T. Y. (1976) *Biochemistry 15*, 5467–5473.
Udgaonkar, J. B., & Baldwin, R. L. (1988) *Nature 335*, 694–699.
Weissman, J. S., & Kim, P. S. (1991) *Science 253*, 1386–1393.
Wood, L. C., White, T. B., & Nall, B. T. (1988) *Biochemistry 27*, 8562–8568.
Wu, L., Laub, P. B., Elöve, G. A., Carey, J., & Roder, H. (1993) *Biochemistry 32*, 10271–10276.